

# Comparing Surfactant Structures at “Soft” and “Hard” Hydrophobic Materials: Not All Interfaces Are Equivalent

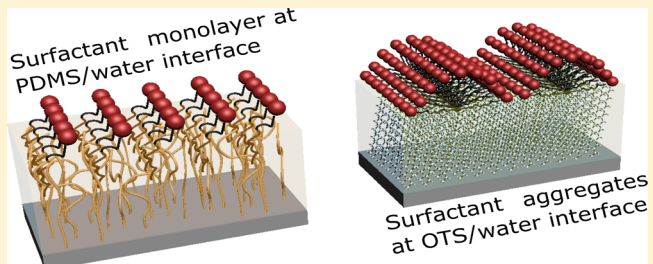
Zengyi Wei,<sup>†</sup> Stefania Piantavigna,<sup>‡</sup> Stephen A. Holt,<sup>‡</sup> Andrew Nelson,<sup>‡</sup><sup>§</sup> Patrick T. Spicer,<sup>†</sup><sup>§</sup> and Stuart W. Prescott<sup>\*,†</sup><sup>§</sup>

<sup>†</sup>School of Chemical Engineering, UNSW Sydney, Sydney, NSW 2052, Australia

<sup>‡</sup>Australian Nuclear Science and Technology Organisation, Lucas Heights, NSW 2234, Australia

## Supporting Information

**ABSTRACT:** The interfacial structures of a range of amphiphilic molecules are studied with both “soft” and “hard” hydrophobic substrates. Neutron reflection and quartz crystal microbalance with dissipation measurements highlight the differences between the adsorbed structures adopted by sodium dodecyl sulfate (SDS), cetyltrimethylammonium bromide ( $C_{16}$ TAB), and the “AM1” surface active peptide. At the soft siloxane/water interface, small molecular surfactants form loosely packed layers, with the hydrophobic tails penetrating into the oily layer, and an area per surfactant molecule that is significantly less than previously reported for the air/water interface. Neutron reflection measurements, supported by quartz crystal microbalance studies, indicate that for  $C_{16}$ TAB, approximately  $30 \pm 8\%$  of the alkyl tail penetrates into the poly(dimethylsiloxane) (PDMS) layer, whereas  $20 \pm 5\%$  of the alkyl tail of SDS is located in the PDMS. For the engineered peptide surfactant AM1 (21 residues), it was found that one face of the  $\alpha$  helix penetrated into the PDMS film. In contrast, penetration of the surfactant tails was not observed against hard solidlike hydrophobic surfaces made from octadecyltrichlorosilane (OTS) for any of the molecular species studied. At the OTS/water interface,  $C_{16}$ TAB and SDS were seen to adsorb as larger aggregates and not as monolayers. Amphiphilic adsorption (amount, structural conformation) at the PDMS/water interface is shown to be different from that at both the air/water interface and the hard OTS/water interface, illustrating that interfacial structures cannot be predicted by the surfactant packing parameter alone. The bound PDMS layer is shown to be a useful proxy for the oil/water interface in surface and stabilization studies, with hydrophobic components of the molecules able to penetrate into the oily PDMS.



## INTRODUCTION

Many important industrial products, such as detergents, shampoos, and cosmetics, are emulsion-based formulations dependent on the stability of the oil/water interface.<sup>1,2</sup> Emulsions are thermodynamically unstable systems, requiring the addition of amphiphilic molecules that provide an electrostatic or steric barrier at the interface that prevents aggregation and coalescence, thereby achieving the desired end-product properties. To design an emulsion-based formulation, one must select an effective and compatible stabilizer. The stabilizer should meet two criteria: adsorbed molecules must have sufficient coverage at the interface, and they must have strong interactions with the interface. These criteria indicate that suitable amphiphiles must have a strong affinity for the hydrophobic component and must pack densely at the interface (for example, by penetrating into the oil phase). In addition, the assembly of adsorbed molecules at a surface permits tailoring of interfacial properties, offering, for example, bespoke biocompatible stabilizers for use in drug delivery systems.<sup>3</sup> At the solid/liquid interface, amphiphilic structures have been shown to be significant to addressing formulation problems<sup>4,5</sup> and it is reasonable to assume that this

will also be the case for the liquid/liquid interface. The stabilization performance of poly(dimethylsiloxane) (PDMS) oil by commodity surfactants such as cetyltrimethylammonium bromide ( $C_{16}$ TAB) and sodium dodecyl sulfate (SDS) was addressed by Woodward et al.,<sup>6</sup> who reported the formation of PDMS droplets by microfluidic processes was heavily influenced by the choice of surfactant. The engineered peptide surfactant “AM1” has been more recently developed for high-performance nanoscale emulsions,<sup>3</sup> and thus the comparison of  $C_{16}$ TAB, SDS, and AM1 offers structural insights that rationalize the existing intuition held by those skilled in formulating with PDMS.<sup>6,7</sup>

Neutron reflection has shown its strength in the study of interfacial surfactant films, thanks, in part, to the ability to vary the scattering length density (SLD) through isotopic substitution. SLD variations can then permit different parts of the system to be highlighted in successive experiments. In X-ray scattering, however, the SLD varies only weakly between

Received: May 22, 2018

Revised: July 5, 2018

Published: July 12, 2018

the oil, water, and surfactant components and unlike in neutron scattering experiments, the contrast variation approach cannot be employed to obtain richer structural understanding. Significant knowledge of the air/liquid and solid/liquid interfaces has been developed using both neutron and X-ray reflectometry (XRR).<sup>8–10</sup>

Probing conformations at the liquid/liquid interface has proven challenging as it is difficult to see the buried liquid interface,<sup>8,11–13</sup> and so the air/water interface is a common proxy for the oil/water interface. At the air/water interface, SDS and C<sub>16</sub>TAB form densely packed monolayers with the head groups and a small fraction of the hydrocarbon tails is immersed into the water leaving the rest of the tails extended into the air. As the concentration of the surfactant is increased toward the critical micelle concentration (cmc), the alkyl chain becomes more extended.<sup>14,15</sup> It is debatable as to how appropriate it is to extrapolate directly from the air/water interface to the liquid/liquid interface, and thus undertaking measurements at the liquid/liquid interface is desirable.

Direct measurement of structures at the liquid/liquid interface has been attempted, with past attempts to study the interfacial structures using neutron reflection from either thinly spread oil layers or condensed volatile oils on the aqueous phase.<sup>8,11,13</sup> Because of the strong attenuation of the neutron beam through the liquid phase, the oil layer in these studies must be very thin and it is both time consuming and technically challenging to achieve ultrathin, uniform layers. Zarbakhsh and co-workers successfully used a frozen oil layer design combined with neutron reflection to probe interfacial structures of various surfactants at the oil/water interface.<sup>12,16–18</sup> These studies revealed that surfactants at the liquid/liquid interface have different conformations compared to those at air/liquid and solid/liquid interfaces.

Compared with the air/water interface, the area per molecule of SDS and C<sub>16</sub>TAB is much larger at the hexadecane/water interface, indicating that the adsorbed amount is less.<sup>12</sup> The ionic surfactants are reported to form disordered and loosely packed monolayers at the interface, with the alkyl chains adopting less tilted conformation than that at the air/water interface.<sup>19</sup>

The limited knowledge of molecular structures at the liquid/liquid interface has also been built upon X-ray scattering measurements where the high intensity that is available ameliorates the significant attenuation of the beam by the sample.<sup>20–22</sup> Scoppola and co-workers combined X-ray and neutron reflectivity measurements to determine liquid/liquid interfacial structures during solvent extraction and showed that the combination of two techniques takes the advantage of contrast variation in both scattering and electron density and therefore it is possible to map out interfacial structures as well as potential energy of the system.<sup>13,23,24</sup> Further structural information obtained from other techniques, such as sum-frequency spectroscopy and surface potential at the oil/water interface, is indirect and can only give partial structural information such as adsorbed layer thickness.<sup>19,25</sup>

Here, we report a model oil/water interface that provides an “anchored” oil film on which traditional surface characterization experimental approaches can be used. We utilize covalently anchored PDMS chains as an immobilized oil layer for adsorption studies at the oil/water interface. The films can be prepared on large silicon blocks, creating large flat areas for study that are suitable for neutron reflection. We also prepare films on quartz crystal microbalance (QCM) sensors for study

of the interfacial mass adsorption. Atomic force microscopy (AFM), X-ray, and neutron reflection measurements show that the PDMS surface is suitably smooth and receptive to surfactants. In this study, we report interfacial structures of the amphiphilic molecules at this soft interface and compare these structures to a hard hydrophobic surface.

To illustrate the generality of our approach, we report studies of surfactants from different classes: anionic (SDS), cationic (C<sub>16</sub>TAB), and a 21 residue peptide that was designed as a surfactant (AM1). The ionic surfactants are commercially used in home care products, and their interfacial structures are well studied at the air/water interface and other hydrophobic solid/water interfaces. The new designer surfactant AM1 (Ac-MKQLADSLHQLARQVSRLHEA-CONH<sub>2</sub>) is stimuli-responsive and has interesting switchable mechanical properties.<sup>26</sup> AM1 is an amphipathic peptide, which consists of repeating hydrophobic residues methionine (M), leucine (L), and valine (V), and has been shown to readily adsorb at the oil/water interface as an emulsifier for tailored nanoemulsion synthesis for antigen delivery.<sup>27</sup> Like the ionic surfactants, the adsorption behavior of AM1 at the air/water interface has been studied previously.<sup>3,14,28</sup>

## EXPERIMENTAL SECTION

Dihydroxyl-terminated PDMS (25 cSt, Aldrich product number 481939,  $\overline{M}_n = 550 \text{ g mol}^{-1}$ ), hydrogenated sodium dodecyl sulfate (h-SDS), hydrogenated cetyltrimethylammonium bromide (h-C<sub>16</sub>TAB), heptane (anhydrous, 99%), toluene (analytical, 99%), and hydrogenated octadecyltrichlorosilane (OTS) were purchased from Sigma-Aldrich and used without further purification. Deuterated SDS (*d*-SDS), deuterated octadecyltrichlorosilane (*d*-OTS), and deuterated C<sub>16</sub>TAB (*d*-C<sub>16</sub>TAB) were obtained from the ISIS Isotope Facility. Surfactants were dissolved in Milli-Q water or D<sub>2</sub>O (supplied by Australian Nuclear Science and Technology Organisation (ANSTO)) to desired concentration.

AM1 was purchased from China Peptides. The AM1 purity was 99.28% (determined by reversed-phase high-performance liquid chromatography). AM1 solutions were prepared in 4-(2-hydroxyethyl)-1-piperazine ethanesulfonate (HEPES, ICN Biomedical) buffer solution at pH 7.0 with 80  $\mu\text{M}$  Zn<sub>2</sub>SO<sub>4</sub>.

**PDMS Brush Synthesis and Characterization.** A thin PDMS brush layer was assembled on silicon wafers (10 mm thick  $\times$  100 mm diameter, EL-CAT Inc.) and quartz crystal microbalance with dissipation (QCM-D) sensors by reacting a hydroxyl group on the PDMS with silanol groups on the silicon surface at high temperature to form a covalent linkage.<sup>29</sup> Similar to previous PDMS grafting methods,<sup>29</sup> the substrates were rinsed with ethanol, acetone, and Milli-Q water and dried under a gentle flow of nitrogen gas before surface activation. After cleaning, the substrates were treated with air plasma (Harrick Plasma PDC-32G) for 40 s on a high radio frequency level to saturate the native oxidized layer with hydroxyl groups. Hydroxyl-terminated PDMS was diluted to 2% (v/v) in heptane and then spin-coated onto the substrates at 4000 rpm for 90 s. The PDMS-coated substrates were then thermally annealed at 170 °C for 6 h in a vacuum oven. Excess unanchored PDMS was removed by rinsing the surface with heptane.

Analysis of the as-formed PDMS films was undertaken by the following techniques. X-ray reflectometry (XRR) measurements were performed in air using a Panalytical X'Pert Pro reflectometer (Cu K $\alpha$ , 1.54 Å). Contact angles were measured using an optical tensiometer (Attension tensiometer, Biolin Scientific). A 4  $\mu\text{L}$  Milli-Q water droplet was placed onto the surface, and the image of the drop was captured and analyzed. The PDMS surface was also characterized in air using a Multimode MM8 AFM with a NanoScope V controller (Bruker) operating in TappingMode. Images were collected over a 500 nm  $\times$  500 nm region at a 0.5 Hz scan rate with a ScanAsyst-Air

**Table 1.** Scattering Lengths and Scattering Length Densities of Surfactant Components

component	scattering length, $\sum b$ ( $\times 10^{-5}$ Å)	SLD, $\rho$ ( $\times 10^{-6}$ Å $^{-2}$ )	component	scattering length, $\sum b$ ( $\times 10^{-5}$ Å)	SLD, $\rho$ ( $\times 10^{-6}$ Å $^{-2}$ )
h-SDS	15.98	0.34	h-C <sub>16</sub> TAB	-14.6	-0.26
d-SDS	276.23	5.36	d-C <sub>16</sub> TAB	422.65	6.9
C <sub>12</sub> D <sub>25</sub>	244.1	7.2	C <sub>16</sub> D <sub>33</sub>	324.8	7.1
C <sub>12</sub> H <sub>25</sub>	-13.7	-0.4	C <sub>16</sub> H <sub>33</sub>	-1.7	-0.37
NaSO <sub>4</sub>	29.7 <sup>a</sup>	3.5 <sup>a</sup>	N(CD <sub>3</sub> ) <sub>3</sub> <sup>+</sup> Br <sup>-</sup>	95.7 <sup>b</sup>	6.6 <sup>b</sup>
AM1 in H <sub>2</sub> O	535.2	1.7	AM1 in D <sub>2</sub> O	897.2 <sup>c</sup>	2.85

<sup>a</sup>Values taken from ref 39. <sup>b</sup>Values taken from ref 40. <sup>c</sup>Exchange of labile hydrogens with 100% D<sub>2</sub>O was considered to be complete.

cantilever (Bruker). The roughness of the surface was estimated using the Gwyddion scanning probe microscopy software.<sup>30</sup>

The brush dimensions are parameterized in terms of an overall grafting density,  $\sigma$ , representing the number of molecules per unit area, and a reduced tethered density,  $\sum$ , representing the degree of crowding on the surface. For a dry brush thickness,  $h$ , bulk PDMS density,  $D$ , and number average molecular weight,  $M_n$ ,  $\sigma = hDN_A/M_n$ . The reduced tethered density,  $\sum = \sigma\pi R_g^2$ , where  $R_g$  is the radius of gyration of the PDMS chain;<sup>31</sup>  $\sum < 1$  indicates the mushroom regime, whereas  $\sum > 5$  indicates the strongly stretched brush regime.

Self-assembled monolayers (SAMs) of OTS were prepared on the silicon wafers and QCM-D sensors. After cleaning and plasma activation as above, the substrates were immersed into 0.1% (v/v) OTS/toluene solutions for 15 min under ambient conditions. Excess unbound OTS was removed by rinsing with excess toluene. The OTS SAMs were cured at 60 °C in an oven for an hour. The OTS-modified silicon substrates were examined in air by XRR measurements. The initial XRR measurements indicate the OTS SAM is 23.2 Å, which corresponds to a fully extended length of OTS molecules (see the Supporting Information).

**Neutron Reflectometry (NR) Measurements and Data Analysis.** The NR measurements were performed on the Platypus reflectometer at ANSTO (Sydney, Australia).<sup>32</sup> Reflectivity profiles were measured at two incident angles, typically 0.8 and 3.3° per data collection, corresponding to a  $Q$ -range of ca. 0.01–0.3 Å $^{-1}$ . The instrument resolution ( $\Delta Q/Q$ ) was 0.05, with a beam footprint on the sample of 30 × 50 mm $^2$ . Direct beam transmission runs were collected with corresponding collimation slits. Samples were measured in a standard solid/liquid cell environment with injection ports to permit solvent changes. Samples were allowed to reach adsorption equilibrium for 20 min following injection of the surfactant solution, and then reflectivity profiles were measured at 22 ± 1 °C. Copious amounts of water were flushed through the sample cell when changing surfactants, with the washing protocol informed by the QCM experiments and desorption of the previous surfactant confirmed by neutron reflectometry.

The concentration of SDS and C<sub>16</sub>TAB solutions was 8 and 1 mM, respectively; these concentrations are approximately the critical micelle concentration of the surfactant so that a measurable surface excess is expected at the interface.<sup>33,34</sup> The presence of micelles is also understood to ameliorate the effects of surfactant hydrolysis on the surface structures,<sup>35</sup> permitting the as-supplied surfactants to be used directly. The AM1 concentration used in this study (0.1 mg mL $^{-1}$ ) corresponds to 40 μM (1/10 of the concentration used for nanoemulsions<sup>36</sup>). The scattering length and molecular volume of AM1 were calculated on the basis of its primary amino acid sequence, and a 100% exchange of labile hydrogen between AM1 and D<sub>2</sub>O was taken into account.<sup>37</sup> SDS, C<sub>16</sub>TAB, and AM1 structures were measured by NR at the same concentrations for both the PDMS/water and OTS/water interfaces. Reflectivity was measured against D<sub>2</sub>O solutions for the hydrogenated surfactants and H<sub>2</sub>O solutions for the deuterated surfactants.

The reflectivity profiles obtained in this study were analyzed using a general optical matrix model in the MOTOFIT suite,<sup>38</sup> with a series of thin slabs representing the scattering length density profile normal to the interface. The scattering length and scattering length density of components used in this study are summarized in Table 1. Each layer is defined by layer thickness ( $t$ ), layer SLD ( $\rho$ ), solvent penetration

( $\phi_{\text{sol}}$ ), and interfacial roughness ( $r$ ). Reflectivity data sets from different contrasts were simultaneously refined with parameters, including surfactant layer thickness ( $t$ ), interfacial roughness ( $r$ ), and solvent penetration, joined in a single co-refined model. By undertaking co-refinement with a contrast variation data set, the number of free parameters is substantially reduced and the discriminating power of the technique is improved. Model selection was undertaken on the basis of physically reasonable structures and informed by previous air/water and AFM studies; reduced  $\chi^2$  values permitted inappropriate models to be rejected. The sensitivity of the model to each of the fitting parameters was estimated by  $\chi^2$  mapping, with a 5% deviation from the global minimum  $\chi^2$  value.

From the fitted model parameters, properties of the adsorbed molecules were determined. The overall SLD of the interfacial surfactant/water layer is a volume fraction weighted average of the SLDs of the surfactant,  $\rho_{\text{surf}}$  and solvent,  $\rho_{\text{sol}}$  SLDs

$$\rho = (1 - \phi_{\text{sol}})\rho_{\text{surf}} + \phi_{\text{sol}}\rho_{\text{sol}} \quad (1)$$

where  $\phi_{\text{sol}}$  is the volume fraction of the solvent that penetrates into a layer. Similarly, the area occupied by each surfactant molecule,  $A_s$ , can then be calculated from the molecular volume  $V_m = A_s t$  for a molecular length  $t$ , where the molecular volume is obtained from the experimental data and the standard relationship between the scattering lengths of each atom,  $b_i$ , and SLD

$$\rho = \frac{\sum_i n_i b_i}{V_m} \quad (2)$$

**QCM-D Adsorption Measurements.** Surfactant adsorption at the PDMS/water and the OTS/water interfaces was measured using a quartz crystal microbalance E4 system with dissipation monitoring (Q-Sense AB, Gothenburg, Sweden). The QCM-D instrument measures relative changes to the resonance frequency ( $\Delta f$ ) and energy dissipation ( $\Delta D$ ) of a sensor chip over the course of the experiment. This study used silicon dioxide-coated sensors (QSX303) modified by PDMS and OTS, as described above. The fundamental resonance frequency of the chip is 5 MHz. This fundamental frequency was not considered because of its high sensitivity to the bulk solution changes; the 3rd, 5th, 7th, 9th, and 11th harmonics of this natural frequency were used instead to simultaneously record  $\Delta F$  and  $\Delta D$  as a function of time. From  $\Delta F$ , it is possible to calculate the change in mass on the sensor chip through the Sauerbrey equation<sup>41</sup>

$$\Delta m = -\frac{\Delta F}{n} C \quad (3)$$

in which  $C$  (17.7 ng cm $^{-2}$  at 5 MHz) is the mass sensitivity constant and  $n$  (1, 2, 3,...) is the overtone number. Structural changes of the material deposited were revealed by variations in  $\Delta D$ , which is the ratio of energy loss to energy stored in the system. The original data were processed in QTools (Q-Sense) before being exported for further analysis. All experiments were conducted at a temperature of 25 ± 0.5 °C and repeated at least twice, showing excellent reproducibility.

In each experiment, a solution of surfactant was flushed over the surface of a sensor chip modified with a layer of PDMS or OTS (flow rate 0.1 mL min $^{-1}$ ). Once the flow ceased, the solution was left to equilibrate until the frequency stabilized and then the chamber was rinsed with HEPES buffer or water to remove any unbound material.

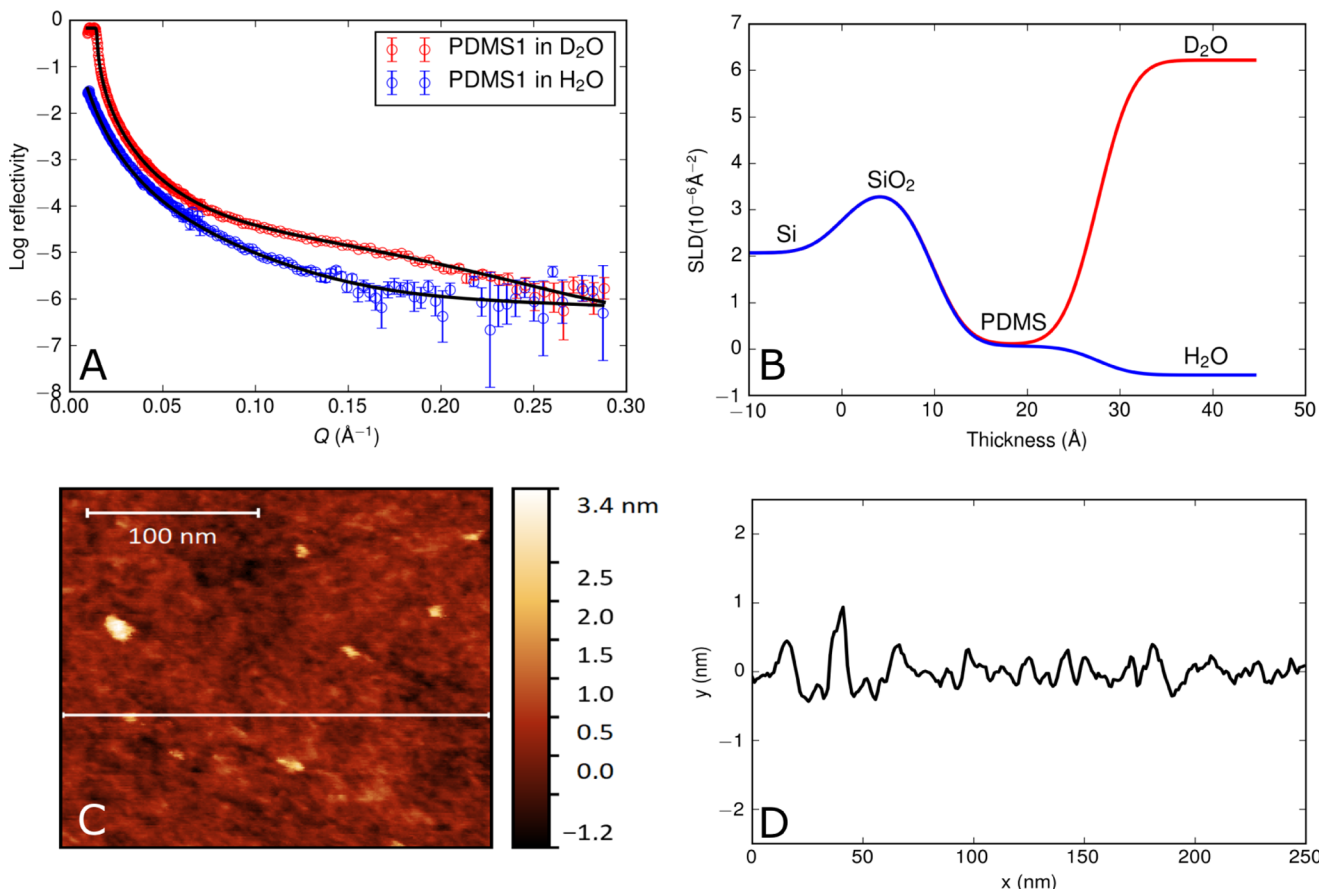


**Figure 1.** NR and AFM characterization of the PDMS coating. (A) Reflectivity profiles of PDMS measured in  $\text{D}_2\text{O}$  (red) and  $\text{H}_2\text{O}$  (blue). Black line represents the best fitting of the two-layer model. (B) Corresponding SLD profiles for the model used in (A). (C) AFM image and height profile of the PDMS layer on a silicon substrate. (D) Corresponding height profile analysis of the AFM image gives  $6 \text{ \AA}$   $R_q$  value. A second PDMS surface can be seen in Figure S2.

Surfactant concentrations were the same as those used for the NR measurements above.

## RESULTS AND DISCUSSION

**PDMS Brush Characterization.** Examination of the PDMS films showed that these layers were hydrophobic, thin, smooth, and suitable for NR studies. The static water contact angle on the PDMS-modified substrates was  $98 \pm 3^\circ$ , demonstrating the oily nature of the surface; given that the surface was formed from a dihydroxyl-terminated PDMS, the high contact angle indicates that the silicone functionality dominates the interface and that the hydroxyl moiety is not pushed to the surface. XRR indicated a slight sample-to-sample variation in thickness; the thickness of the PDMS layer ranged between  $14.0 \pm 1.3$  and  $17.8 \pm 0.6 \text{ \AA}$  (see the Supporting Information for further details). These PDMS films are, therefore, sufficiently thick that the tail of a small ionic surfactant could be expected to penetrate into the oil if that is the favorable conformation; partitioning and swelling studies indicate that small alkanes are able to penetrate PDMS materials.<sup>42</sup> The contour length of the  $\text{C}_{16}\text{TAB}$  studied here is approx  $18 \text{ \AA}$ .<sup>14,43,44</sup> The roughness of the PDMS layer was around  $3.0 \text{ \AA}$ .

Neutron reflectivity profiles of the PDMS-coated silicon blocks against both  $\text{D}_2\text{O}$  and  $\text{H}_2\text{O}$  were acquired (Figure 1A) and co-refined with a two-layer model that consists of a layer of native oxide ( $\text{SiO}_2$ ) and a thin layer of PDMS. The resultant

models showed that the SLD of the PDMS layer was not dependent on the solvent used, indicating that the PDMS did not have significant porosity or large defects (Figure 1B); the fitting parameters for the bare PDMS are summarized in Table S1. Topographic profiles of a replicate PDMS layer were measured by AFM (Figure 1C), and the height profiles of the PDMS brush gave a root-mean-square roughness  $R_q = 6 \text{ \AA}$  (Figure 1D). The occasional  $50 \text{ \AA}$  wide bumps seen in the image were attributed to long-chain impurities of the hydroxy-terminated PDMS, making the occasional “mushroom” conformer sitting above the brush. The AFM phase image of the brush layer indicated uniform coverage without large pin holes (Figure S3), in line with the porosity result from NR.

The thickness of the brush layer from NR and XRR measurements was consistent with the overall grafting density of the PDMS brush, giving  $\sigma = 1.85 \text{ chains nm}^{-2}$  (Figure 1) and  $1.46 \text{ nm}^{-2}$  (Figure S2), respectively, for the two surfaces reported here. The reduced tethered densities were estimated to be 13 and 10, respectively, indicating that the chains are stretched and crowded within these brushes.<sup>31</sup> Thicker PDMS films have also been produced using higher molecular weight hydroxyl-PDMS precursor material, with a  $5000 \text{ g mol}^{-1}$  PDMS chain, producing  $30 \text{ \AA}$  thick layers that we will describe in detail in a future publication.

**Ionic Surfactant Structures at the PDMS/Water Interface.** The QCM-D study revealed the dynamics of the  $\text{C}_{16}\text{TAB}$  and SDS adsorption/desorption at the PDMS and

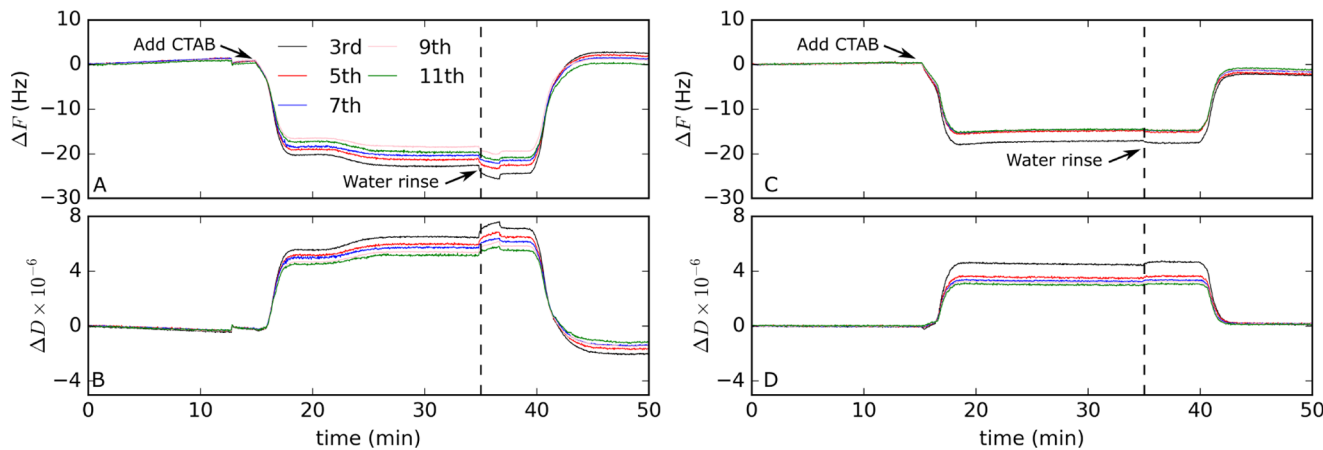


**Figure 2.** Representative curves of (A) frequency shift of 1 mM  $C_{16}TAB$  measured with PDMS-modified QCM-D sensors. (B) Corresponding dissipation changes as a function of time. (C) Frequency shift of 1 mM  $C_{16}TAB$  measured by OTS-modified QCM-D sensors. (D) Corresponding dissipation changes as a function of time.

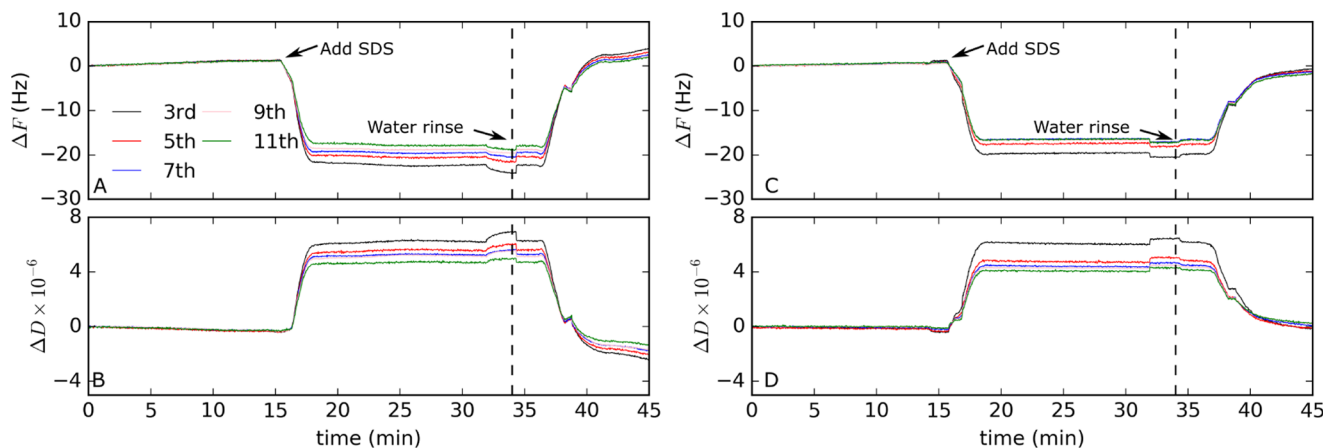


**Figure 3.** Representative curves of (A) frequency shift of 8 mM SDS measured by PDMS-modified QCM-D sensors. (B) Corresponding dissipation changes as a function of time. (C) Frequency shift of 8 mM SDS measured by OTS-modified QCM-D sensors. (D) Corresponding dissipation changes as a function of time.

OTS interfaces. Immediately after the injection of  $C_{16}TAB$  solution in the chamber, a change of frequency and dissipation was observed (Figure 2A,B), suggesting rapid change of surface excess and a fast adsorption of the surfactant at the PDMS interface. A stable baseline is reached at around  $-20$  Hz; however, there is a variation between the lowest- and highest-order harmonics of  $6$  Hz, indicative of a viscoelastic coupling<sup>41</sup> is problematic in the viscoelastic case; however, the apparent adsorbed mass of  $9.7\ \mu\text{mol m}^{-2}$  so obtained is indicative of a significant amount of coupled water and is consistent with the NR results (below). The increase in dissipation additionally indicates that the adsorbed layer is nonrigid (Figure 2B). After rinsing with water, both frequency and dissipation returned to zero, indicating that mass, likely  $C_{16}TAB$ , was removed from the surface. The small spread between the overtones in both frequency and dissipation at the end of the experiment indicate some damage to the surface during the experiment.

Very similar behavior at the PDMS/water interface was observed also for SDS (Figure 3A,B): a fast adsorption resulting in a frequency change of  $-20$  Hz on average, with variation among overtones, suggested a hydrated, viscoelastic layer at the interface. As observed for  $C_{16}TAB$ , the rinse with water removed SDS and although there was a variation in

dissipation, after the rinsing it was less than that seen for  $C_{16}TAB$  on PDMS.

QCM-D demonstrates that these ionic surfactants readily adsorb onto the PDMS layer, as would be expected, and also shows that both adsorption and desorption are fast processes, taking seconds to minutes. At the molecular level, the stationary PDMS layer is seen to be an effective proxy for understanding surfactant behavior at the oil/water interface and kinetic experiments on the adsorption of surfactants and polymers can be undertaken using this proxy.

To further quantify the structure of the surfactant layer at the PDMS/water interface, NR experiments were undertaken. Analysis of NR data requires comparison of the reflectivity predicted by a hypothesized model with the experimentally obtained reflectivity. In these experiments, we seek to distinguish between two possibilities for the location of the surfactant at the surface: a penetration model where the surfactant tails penetrate into the PDMS layer, and an exclusion model where the surfactant tails do not penetrate into the PDMS layer. By co-refining the models with multiple contrasts (h-surfactant in  $D_2O$  and d-surfactant in  $H_2O$ ), the neutron reflection experiment offers greater discriminating power for this system and it becomes possible to distinguish between the penetration and exclusion models.

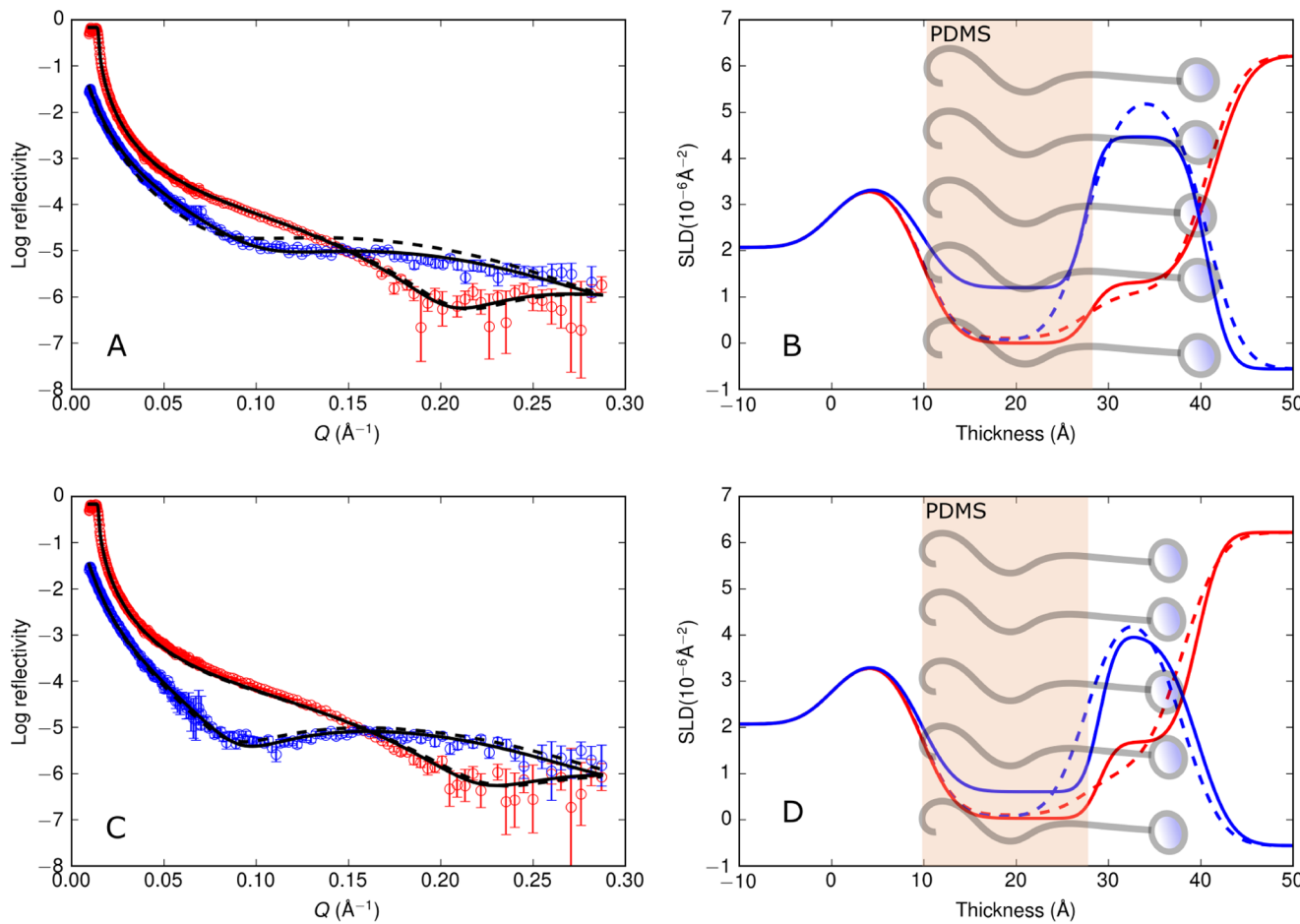


**Figure 4.** Reflectivity profiles and corresponding SLD profiles from the modeling. h-Surfactants measured in  $\text{D}_2\text{O}$  are in red. d-Surfactants measured in  $\text{H}_2\text{O}$  are in blue. Dashed lines represent the exclusion model, and solid lines represent the penetration model. Upper row: 1 mM  $\text{C}_{16}\text{TAB}$  adsorbed at the PDMS/water interface. Lower row: 8 mM SDS adsorbed at the PDMS/water interface.

$\text{C}_{16}\text{TAB}$ . NR shows that the ionic surfactants  $\text{C}_{16}\text{TAB}$  and SDS readily adsorb to the PDMS surfaces forming molecular-dimensioned layers. Figure 4A shows the reflectivity profiles from layers formed from 1.0 mM solutions of h- $\text{C}_{16}\text{TAB}$  in  $\text{D}_2\text{O}$  (red) and d- $\text{C}_{16}\text{TAB}$  in  $\text{H}_2\text{O}$  (blue) as well as the model SLD profiles (Figure 4B). The hydrated surfactant layer that is formed at the PDMS/water interface is too thin (13 Å) to be derived from adsorbed micelles or hemimicelles (upward of 30 Å).<sup>45</sup>

The simplest model used was the exclusion model where a layer of surfactant and solvent was placed adjacent to the PDMS. The exclusion model is unable to satisfactorily fit the NR data, with the best fit achievable with this model shown as a dotted line in Figure 4A. Using separate layers for the surfactant head and tail offered no improvement to the fit, given the minimal contrast between head and tail and the roughness of the surface.

For the penetration model, where the hydrocarbon tails of the surfactant are permitted to penetrate into the PDMS layer, the SLD of the hydrophobic surface layer is the volumetric mixture of the bound PDMS and part of the alkyl chain of the surfactant tail; the remainder of the surfactant tail and the surfactant head were modeled as a solvated layer above the PDMS surface. The model is constrained to ensure equal numbers of surfactant heads and tails are present. The SLD that is obtained from these data therefore provides a means to

estimate the proportion of the hydrocarbon tail penetrating into the PDMS layer (see the Supporting Information).

In the case of  $\text{C}_{16}\text{TAB}$  at the PDMS/water interface, the penetration model provided the best fit for both d- $\text{C}_{16}\text{TAB}$  and h- $\text{C}_{16}\text{TAB}$  contrasts. The effect of penetration is seen in the SLD profile (Figure 4B), where the penetration model (blue solid line) is readily distinguishable from the exclusion model (blue dashed line). The reduced  $\chi^2$  value changed from 6.3 for the exclusion model to 0.7 for the penetration model. Table 2 summarizes the fitting parameters used in the penetration model; briefly, a portion of the tail is seen to mix into the

**Table 2. Fitting Results of PDMS in  $\text{D}_2\text{O}$  and  $\text{C}_{16}\text{TAB}$ , SDS, and AM1 Adsorbed at the PDMS/Water Interface<sup>a</sup>**

Solution	Layer	Tail vol frac $\phi_{\text{tail}} (\%)$	Layer thickness <sup>a</sup> $t (\text{\AA})$	Area per molecule $A_s (\text{\AA}^2)$
$\text{D}_2\text{O}$	PDMS1	-	$17.8 \pm 0.6$	-
	PDMS1+tail	16	$18 \pm 2.4$	52
$\text{C}_{16}\text{TAB}$	tail+head+water	67	$13 \pm 0.4$	-
	PDMS1+tail	8	$19.3 \pm 1.5$	50
SDS	tail+head+water	77	$10.7 \pm 0.8$	-
	PDMS1+tail	7.3	$18.3 \pm 0.7$	438.1
$\text{D}_2\text{O}$	PDMS2	-	$14 \pm 1.3$	-
	PDMS2+tail	50	$14.4 \pm 0.7$	-
AM1	tail+head+water	-	-	-
	PDMS2+tail	-	-	-

<sup>a</sup>Confidence interval indicates sensitivity of the model to parameter.

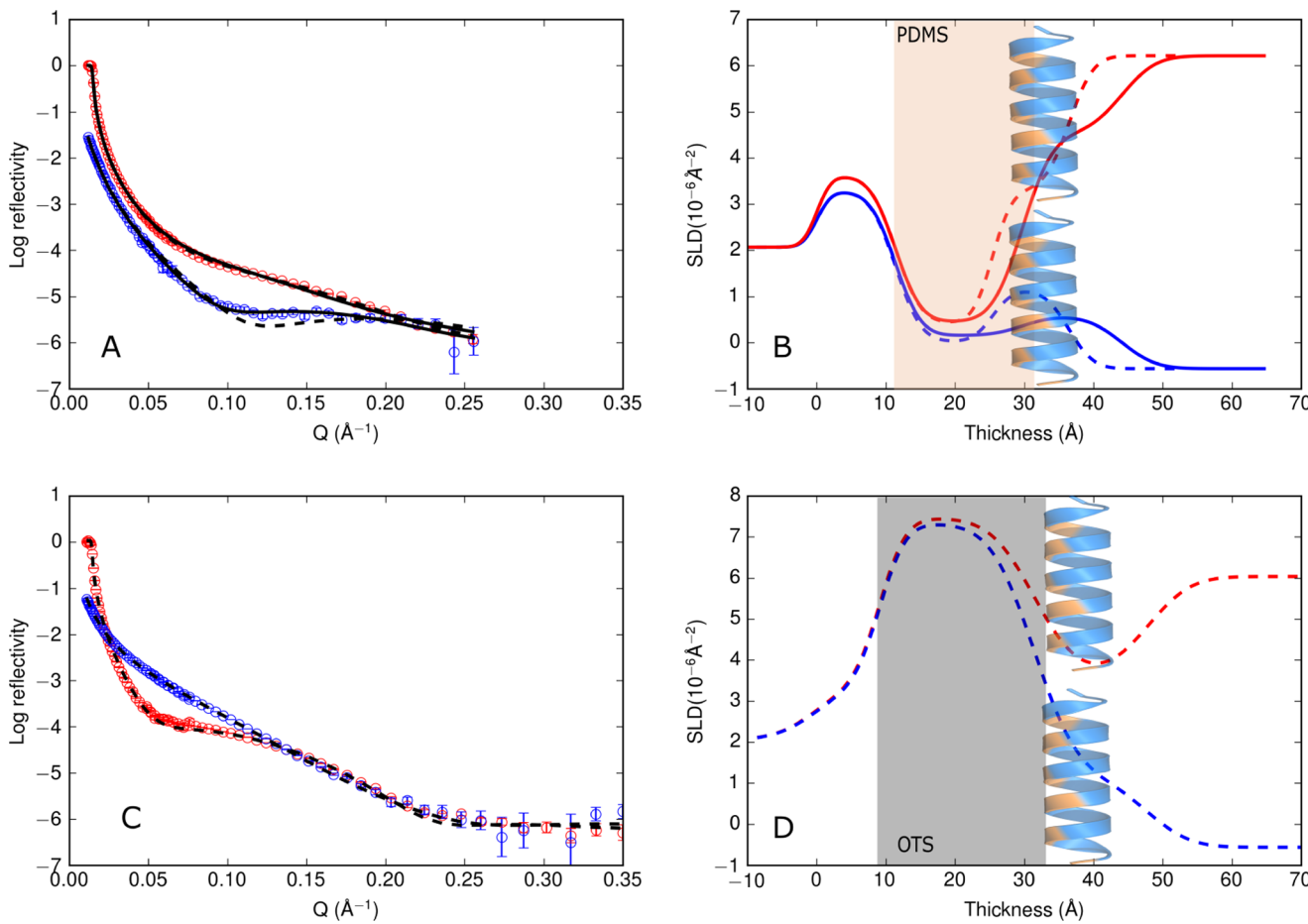


**Figure 5.** Reflectivity profiles and corresponding SLD profiles for  $0.1 \text{ mg mL}^{-1}$  AM1 solution, as measured in  $\text{D}_2\text{O}$  (red) and  $\text{H}_2\text{O}$  (blue). Dashed lines represent the exclusion model, and solid lines represent the penetration model. Upper row:  $0.1 \text{ mg mL}^{-1}$  AM1 adsorbed at the PDMS/water interface. Lower row:  $0.1 \text{ mg mL}^{-1}$  AM1 adsorbed at the OTS/water interface.

PDMS layer while a substantial portion of the tail is found in the solvated layer.

Within the  $18 \text{ \AA}$  thick  $\text{C}_{16}\text{TAB}$ -tail/PDMS layer, the volume fraction of the hydrocarbon surfactant tails is 16%. The model indicates that  $\text{C}_{16}\text{TAB}$  adsorbed at PDMS/water interface and can penetrate into the soft PDMS layer, with  $33 \pm 8\%$  of the alkyl chain immersed in the PDMS; further details of this analysis are contained in the [Supporting Information](#).

Given that the PDMS layer is approximately the same thickness as the contour length of the surfactant tail and yet the majority of the tail remains excluded from the PDMS, these results also indicate that the favorable conformation of the  $\text{C}_{16}\text{TAB}$  chain is not to penetrate fully into the PDMS. While penetration of the hydrocarbon tail into OTS at the OTS/water interface was reported by Penfold et al.,<sup>46</sup> the OTS layer used in the study was very rough and had a low surface coverage, giving 60% solvent penetration into the OTS layer. In comparison with previous work on rough or patchy layers, the PDMS films reported here contain little water and serve as an excellent proxy for studying the oil/water interface, providing a significant advancement over previous work.

QCM-D indicated that a viscoelastic layer with significant coupling of solvent was present on the surface; NR identifies this layer as a layer of solvated surfactant. The thickness of the solvated solvent layer containing some of the surfactant tail and the surfactant head was found to be  $13 \text{ \AA}$ . The SLD of this layer indicates that it is comprised of 67% of the volume of the

surfactant tail (i.e.,  $\text{C}_{16}\text{H}_{34}$ ) and the surfactant head and the remainder is water. Considering the electrostatics of this layer, it is clear that Coulombic repulsions would be reduced if the surfactant heads were diluted through this layer and so the surfactant tails would be drawn out of the oil to form a layer with heads, tails, and solvent. Further, image charge repulsion, wherein the dielectric discontinuity across the PDMS/water interface generates a same-signed image charge within the PDMS that repels the surfactant head, would prevent the whole alkyl tail from inserting into the PDMS.<sup>47</sup> Similar phenomena have been reported for the adsorption of polyelectrolytes, where the polyelectrolyte was depleted from the adsorbed surface due to image charge repulsion.<sup>48</sup>

The surface excess of  $\text{C}_{16}\text{TAB}$  was calculated to be  $3.2 \mu\text{mol m}^{-2}$ , corresponding to an area per molecule ( $A_s$ ) of  $52 \text{ \AA}^2$ . The  $A_s$  found here for the PDMS/water interface is slightly higher than that at the air/water interface, where the typical range is  $40\text{--}45 \text{ \AA}^2$ .<sup>14,43,44</sup> However, this is in agreement with other attempted hydrophobic liquid/water interface studies;<sup>12,49</sup> Lu et al. reported  $A_s = 52 \text{ \AA}^2$  for  $\text{C}_{16}\text{TAB}$  at the dodecane/water interface,<sup>49</sup> and Zarbakhsh et al. reported that the value increases to  $124 \text{ \AA}^2$  at the hexadecane/water interface.<sup>12</sup> Consistent with these previous reports, these data indicate a thin monolayer of surfactant is present at the interface and even though the measurement temperature is close to the Krafft temperature of  $\text{C}_{16}\text{TAB}$ , crystallite surface structures are not observed.

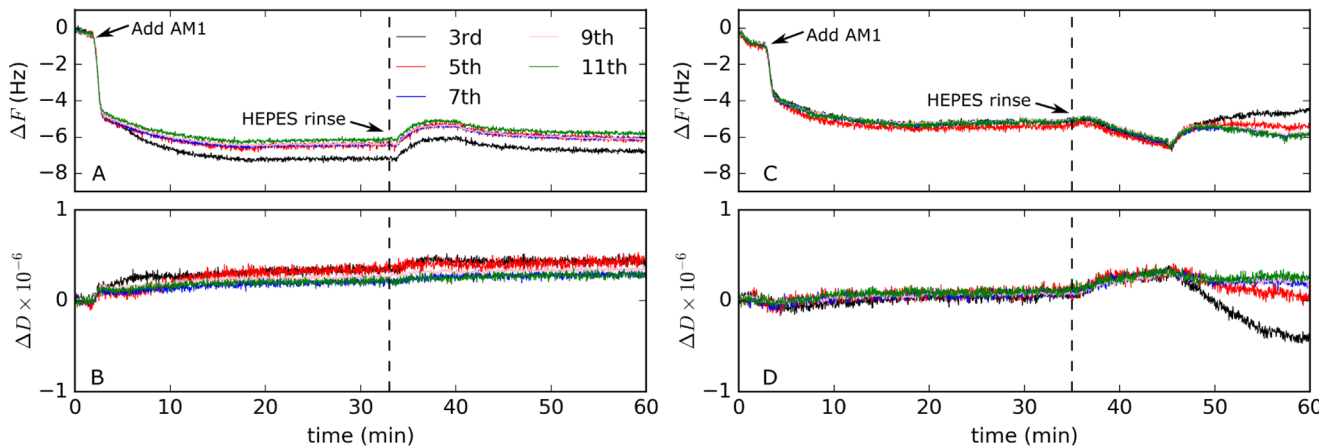


**Figure 6.** Representative curves of (A) frequency shift of  $0.1 \text{ mg mL}^{-1}$  AM1, followed by HEPES buffer rinsing measured by PDMS-modified QCM-D sensors. (B) Corresponding dissipation changes as a function of time measured by PDMS-modified QCM-D sensors. (C) Frequency shift of  $0.1 \text{ mg mL}^{-1}$  AM1, followed by HEPES buffer rinsing measured by OTS-modified QCM-D sensors. (D) Corresponding dissipation changes as a function of time measured by OTS-modified QCM-D sensors.

These results suggest that the surfactant alkyl chain interacts with PDMS and forms an adsorbed layer but that the PDMS layer has a substantial effect on the surfactant. The area per molecule in this layer is higher than that at the air/water interface and coupled with the QCM-D data (above) showing that the surfactant is quite labile, hints at the reportedly poor performance of  $C_{16}\text{TAB}$  for PDMS applications.<sup>6,7</sup>

SDS. NR for SDS adsorbed at the PDMS/water interface is shown in Figure 4C. The exclusion and penetration models (as described above) were once again used to investigate these data. Although both the exclusion and penetration models can be made to give satisfactory fits to the data, as shown in Figure 4D, acceptable fits from the exclusion model require an unphysical swelling of the PDMS layer, which is inconsistent with the exclusion model. The conclusion is that penetration of the surfactant tail into the PDMS film is most likely. We note that the depicted uniform concentration of surfactant tail in the PDMS layer could be treated with a more sophisticated concentration gradient at the expense of further complexity in the structural model for the interface.

The penetration model indicates that  $20 \pm 5\%$  of the length of the alkyl chain immerses into the PDMS, occupying 8% v/v of the layer (see the Supporting Information for further details of this analysis). Consequently, 80% of the tail and the head region extends into the aqueous phase, forming an 11 Å thick layer that is 23% v/v water. That SDS shows a reduced penetration of the tails into the PDMS in comparison with  $C_{16}\text{TAB}$  can be understood in terms of the hydrophilicity of the two molecules, with  $C_{16}\text{TAB}$  having a much lower cmc and thus a higher propensity to be excluded from the water phase and penetrate the PDMS phase. The difference in hydrophilicity is understood to be based not only on the tail length but also the better stabilization of the anionic head group by surrounding water.

The surfactant  $A_s$  was calculated to be  $50 \text{ \AA}^2$  with a surface excess value of  $3.3 \mu\text{mol m}^{-2}$ . The relatively small penetration of the SDS tail into the film indicates that the penetration is not limited by the thickness of the PDMS film. Similar to the  $C_{16}\text{TAB}$  case, the area per SDS molecule is slightly larger than the value at the air/water interface ( $42\text{--}45 \text{ \AA}^2$ ) reported by NR and surface tension measurements.<sup>50,51</sup> The reduced surface coverage of the surfactant compared to that at the air/

water interface is consistent with previous small-angle neutron scattering studies of SDS adsorbed at hexadecane/water interface,<sup>52</sup> as well as at carbon tetrachloride/water and graphite/water interfaces studied by molecular dynamic simulations and NR.<sup>53–55</sup>

**AM1 Structures at the PDMS/Water Interface.** In contrast to commodity surfactants SDS and  $C_{16}\text{TAB}$ , the peptide AM1 is a recently engineered molecule that, while rather surface active, is substantially hydrophilic and has significant secondary structure as an  $\alpha$ -helix; it has previously been postulated that the  $\alpha$ -helix has hydrophilic and hydrophobic sides and that it would sit at the oil/water interface with the helix axis parallel to the interface.<sup>3</sup> Here, we investigated  $0.1 \text{ mg mL}^{-1}$  AM1 adsorption at the PDMS/water interface by NR on a newly PDMS-coated silicon block (Figure 5A). Co-refinement of different contrasts (AM1 in  $D_2\text{O}$  (red) and in  $H_2\text{O}$  (blue)) once more allows the adsorbed layer thickness, area per molecule, and surface excess at the interface to be obtained. The single uniform layer of AM1 on the PDMS (the exclusion model) is unable to match the measured reflectivity. Instead, a penetration model where some fraction of the AM1 penetrates into the PDMS layer was required to adequately fit to the data, with the remaining part of the AM1 molecule exposed to the aqueous phase (solid line in Figure 5A). Including a proximal pure PDMS layer and then an AM1/PDMS mixture did not improve the fits further.

As in studies of emulsions stabilized by AM1, the thickness of the AM1 layer is consistent with the  $\alpha$ -helix sitting flat on oil/water interface, as depicted (the diameter of an  $\alpha$ -helix is about 14 Å).<sup>3</sup> The hydrophobic part of the  $\alpha$ -helix of AM1 is buried into the PDMS layer, comprising about 7% v/v of the PDMS layer. The swelling of the PDMS brush layer from 14 to 18 Å indicates strong favorable interactions between the hydrophobic residues of AM1 and the PDMS chains. The rest of the AM1 molecule extends into the aqueous phase and forms a layer of 14 Å containing 50% v/v associated water. The area per molecule of AM1 calculated from the upper layer is  $438 \text{ \AA}^2$ , and the surface excess is  $0.4 \mu\text{mol m}^{-2}$ . Similar to the earlier finding that the area per molecule was larger at the PDMS/water interface than that previously reported for the air/water interface, it is seen here that the area per molecule

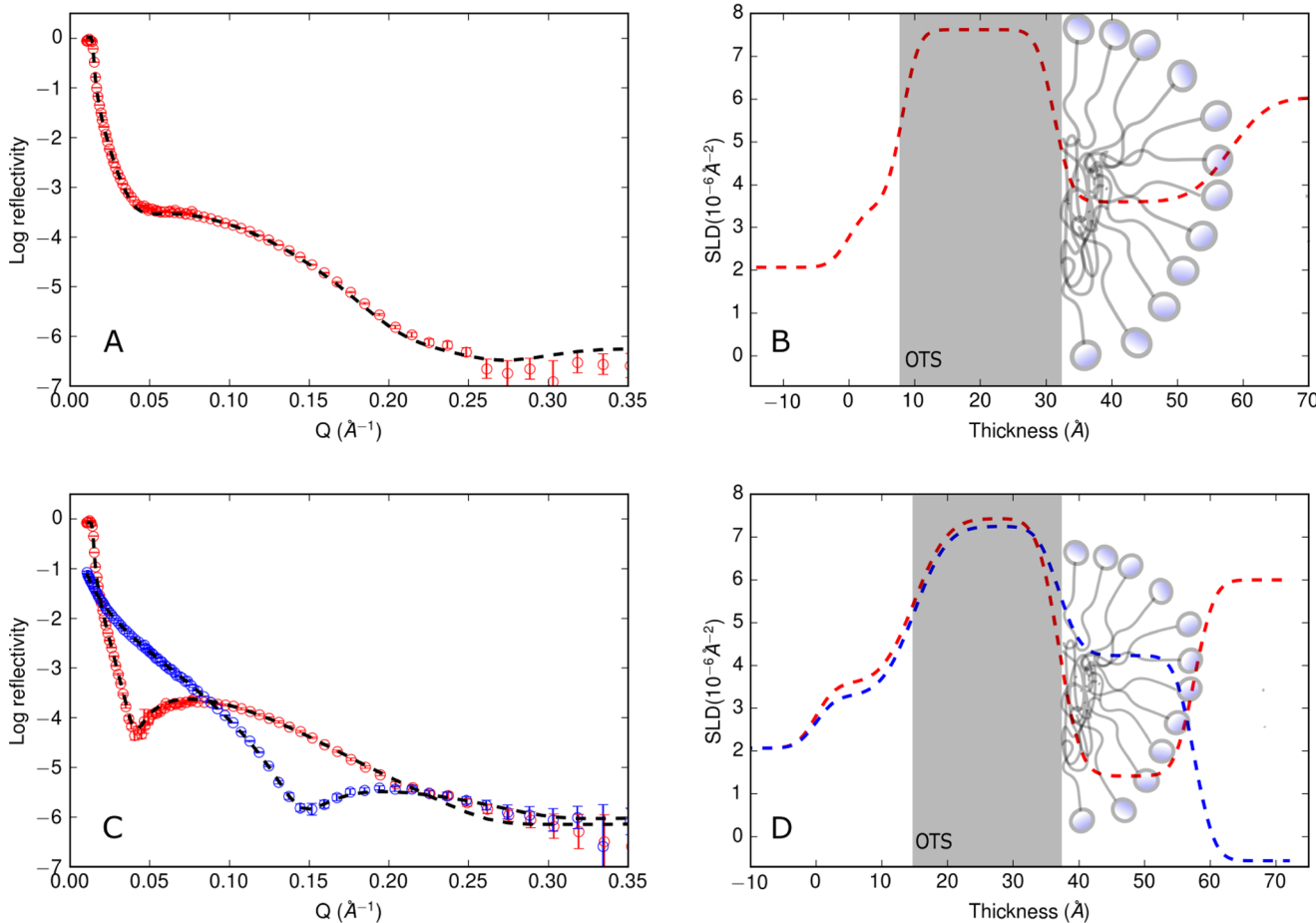


**Figure 7.** Reflectivity profiles and corresponding SLD profiles for the fittings. h-Surfactants measured in  $\text{D}_2\text{O}$  are in red. d-Surfactants measured in  $\text{H}_2\text{O}$  are in blue. Dashed lines represent the uniform layer model, and solid lines represent the penetration model. Upper row: 1 mM  $\text{C}_{16}\text{TAB}$  adsorbed at the OTS/water interface. Lower row: 8 mM SDS adsorbed at the OTS/water interface.

for the AM1 is increased; Middelberg et al.<sup>3</sup> reported the area per molecule of AM1 at the air/water interface was  $380 \text{ \AA}^2$ .

QCM-D data shows that most of the AM1 adsorption occurs quite rapidly, followed by a slow mass increase over about 10 min, reaching a maximum frequency change of  $-6.5 \text{ Hz}$  for all harmonics except the third (Figure 6A). Indeed, the frequency recorded at this harmonic is  $-7.0 \text{ Hz}$ . This difference of  $0.5 \text{ Hz}$  could be an indication of partial penetration into the PDMS layer, as predicted by NR modeling. The small change in frequency upon rinsing with buffer indicates that most of the adsorbed mass remained on the surface. The adsorption of AM1 is therefore largely irreversible, in stark contrast to the  $\text{C}_{16}\text{TAB}$  and SDS data shown above. The dissipation response of AM1 is also notably different to that of  $\text{C}_{16}\text{TAB}$  and SDS, with virtually no change in dissipation and no spread across the harmonics. It is concluded that the AM1 layer is rigidly coupled to the surface. The adsorbed mass was calculated using the method of Rodahl et al.<sup>56</sup> to be  $0.4 \text{ } \mu\text{mol m}^{-2}$ , which is in agreement with the value calculated from NR data.

**Surfactant Structures at the OTS/Water Interface.** Studies of amphiphiles at the solid/liquid interface have historically used OTS self-assembled monolayers as an immobilized hydrophobic surface. The structures of SDS,  $\text{C}_{16}\text{TAB}$ , and AM1 at the OTS/water interface thus provide an interesting comparison with what has been reported here for the PDMS/water interface. Of particular interest is the degree

to which the surfactants can (or cannot) penetrate into the hydrophobic layer, as that is an important factor when considering the suitability of the OTS/water and PDMS/water interfaces as proxies for studying the oil/water interface.

QCM experiments for  $\text{C}_{16}\text{TAB}$  and SDS at the OTS/water interface displayed some similarities to that at the PDMS/water interface. The change in frequency for both  $\text{C}_{16}\text{TAB}$  (Figure 2C,D) and SDS (Figure 3C,D) is similar in magnitude but with much reduced variation between the harmonics (except for the third), indicating the adsorption is a rigid structure with minimal bound solvent. Upon rinsing, the frequency and dissipation returned to the initial values, indicating the OTS layer was not altered by the surfactant adsorption and desorption.

NR showed the *d*-OTS SAM was  $22 \text{ \AA}$  (see Figure S4) with an SLD of  $7.48 \times 10^{-6} \text{ \AA}^{-2}$ , indicating the SAM is a highly ordered crystalline phase with a density of  $0.98 \text{ g cm}^{-3}$  ( $A_s = 24.3 \text{ \AA}^2$ ). At the OTS/water interface, all three surfactants formed a denser layer than at the PDMS/water interface; moreover, a region where the surfactant tail penetrates the hydrophobic layer was not required to achieve good fits to the data, with the exclusion model giving satisfactory fits in all cases (Figures 5C,D and 7); including any amount of penetration of the surfactants into the OTS results in an increased  $\chi^2$  value (see Figure S5). Several surfactants' adsorption on OTS and other silane SAMs has been previously studied by NR.<sup>57,58</sup> In these studies, some penetration of

surfactant tails into the SAM was found. However, the penetration is the result of the partial coverage and the displacement of water molecules by surfactants at the defect sites.

For C<sub>16</sub>TAB, the adsorbed surfactant layer has a thickness of 26.8 Å with 60% v/v water in the layer. This gives an area per molecule (17.5 Å<sup>2</sup>) that is smaller than the C<sub>16</sub>TAB head-group cross-sectional area (35 Å<sup>2</sup>), indicating that the surfactant layer is not a monolayer of C<sub>16</sub>TAB. The adsorbed amount of C<sub>16</sub>TAB was determined to be 3.2 μmol m<sup>-2</sup>. This is in agreement with past studies by AFM showing that at other hydrophobic surfaces, C<sub>16</sub>TAB forms hemimicellar structures with a resultant smaller area per molecule, with the thickness comparable to the radius of a C<sub>16</sub>TAB micelle<sup>45,59–61</sup> and the thickness observed here. Previous NR studies have also reported adsorbed surfactant aggregates (hemispherical, rod-like, or spherical micelles) for the adsorption of C<sub>16</sub>TAB and the chloride equivalent, C<sub>16</sub>TAC, at hard hydrophobic surfaces.<sup>62</sup> As with the existing literature, crystallite surface structures are not observed even though the measurements were performed close to the Krafft temperature.

For SDS, the fitted layer thickness is 21 Å, with 20% v/v water in the surfactant layer. The adsorbed amount was determined to be 5.4 μmol m<sup>-2</sup>. The dimensions and coverage of SDS are consistent with densely packed structures such as the hemicylindrical structures, as suggested by previous studies on hard hydrophobic interfaces.<sup>63,64</sup> These NR data show that both SDS and C<sub>16</sub>TAB adopt substantially different structures, depending on the surface with which they are interacting. At the soft PDMS/water interface, single surfactant layers were observed to be similar in structure to the air/water interface, albeit at lower packing density, whereas at the hard OTS/water interface, surfactant aggregates form.

The interaction of AM1 with OTS (Figure 6C,D) showed some differences compared with grafted PDMS: first, there was a smaller frequency shift (−4 Hz, with all harmonics being superposable), indicating that the AM1 adsorbs without coupling significant water to the surface. Second, the interaction is irreversible as the peptide was not removed by the HEPES rinse (the variation in frequency immediately after the rinse is due to a bulk shift effect). The thickness of an adsorbed AM1 layer was measured to be 16 Å, and there is 27% v/v water within the layer. The area per molecule of AM1 at the interface was calculated to be 265 Å<sup>2</sup> and the surface excess was 0.6 μmol m<sup>-2</sup>, indicating a higher adsorbed amount is found at the OTS/water interface compared to that at the PDMS water interface. Further analysis of the surfactant structures at the OTS/water interface is summarized in Table S2.

## SUMMARY AND CONCLUSIONS

Using a covalently bonded PDMS layer, the interfacial structures of both commodity surfactants (SDS, C<sub>16</sub>TAB) and a boutique surfactant (AM1) have been studied by neutron reflection and quartz crystal microbalance with dissipation. We have demonstrated the first use of a PDMS polymer brush as a proxy suitable for measuring molecular structures at the oil/water interface.

Results show the different adsorption amounts and different structures of surfactants at the PDMS/water interface compared to measurements at the OTS/water interface and previously reported structures at the air/water interface. At the soft PDMS/water interface, surfactants form a loosely packed

monolayer with lower number density compared to that at the air/water interface and only a fraction of the predicted adsorption sites are occupied within the surfactant monolayer. At the hard OTS/water interface, however, surfactant adsorption was seen to proceed via the adsorption of surfactant aggregates rather than forming a monolayer, as observed at the PDMS/water interface.

SDS and C<sub>16</sub>TAB alkyl chains were able to penetrate into the soft PDMS layer but are unable to penetrate the OTS layer. The AM1 peptide forms a thin layer at the PDMS/water interface indicative of the hydrophobic residues of the α-helix penetrating into the PDMS phase. None of the surfactants were able to penetrate into the OTS layer, instead adsorbing to the OTS/water interface without the surfactant tail penetrating into the hydrophobic region.

Importantly, these data illustrate that different hydrophobic substrates lead to different adsorbed structures for amphiphiles; the surfactant structure at the hydrophobe/water interface is not solely determined by the surfactant packing parameter but is dependent upon the molecular interactions of the tail and the hydrophobic material. The surfactant tails are seen to penetrate soft substrates such as PDMS and air, thus permitting monolayer formation, whereas hard, potentially crystalline SAMs such as OTS are seen to exclude the tails and lead to micellar or hemimicellar surface structures. It is presumed that the exclusion of the tails from the OTS layer and also the graphitic layers reported in the literature, results in the formation of the extended surfactant aggregates at these interfaces. Since the nature of the hydrophobic material makes gross changes to the structures of adsorbed surfactants, as well as quantitative changes to the adsorbed amounts, further study of surfactant structures at the oil/water interface cannot rely on hard proxies such as the OTS/water interface but must continue to seek genuine oil/water interfaces such as the PDMS/water interface described here.

## ASSOCIATED CONTENT

### Supporting Information

The Supporting Information is available free of charge on the ACS Publications website at DOI: [10.1021/acs.langmuir.8b01686](https://doi.org/10.1021/acs.langmuir.8b01686).

Further X-ray reflection, neutron reflection, and AFM characterization of the PDMS films; additional fits showing the discounted surfactant penetration or exclusion models against PDMS and OTS ([PDF](#))

## AUTHOR INFORMATION

### Corresponding Author

\*E-mail: [s.prescott@unsw.edu.au](mailto:s.prescott@unsw.edu.au). Phone: +61 (0)2 9385 2641.

### ORCID

Andrew Nelson: [0000-0002-4548-3558](https://orcid.org/0000-0002-4548-3558)

Patrick T. Spicer: [0000-0002-8562-3906](https://orcid.org/0000-0002-8562-3906)

Stuart W. Prescott: [0000-0001-5639-9688](https://orcid.org/0000-0001-5639-9688)

### Notes

The authors declare no competing financial interest.

## ACKNOWLEDGMENTS

The authors acknowledge the support of the Australian Centre for Neutron Scattering, Australian Nuclear Science and Technology Organisation, in providing the neutron research facilities used in this work, proposal PS300, and the National

Deuteration Facility for the use of QCM-D. We thank the Biomedical Imaging Facility and Dr. Celine Heu (UNSW) for the support of AFM measurements. We thank ISIS Deuteration Facility for providing the deuterated materials. We acknowledge financial support from the Australian Government. Z.W. is funded by the Australian Government Research Training Program Stipend Scholarship.

## ■ REFERENCES

- (1) Tadros, T.; Izquierdo, P.; Esquena, J.; Solans, C. Formation and stability of nano-emulsions. *Adv. Colloid Interface Sci.* **2004**, *108–109*, 303–318.
- (2) Tadros, T. F.; Vandamme, A.; Levecke, B.; Booten, K.; Stevens, C. V. Stabilization of emulsions using polymeric surfactants based on inulin. *Adv. Colloid Interface Sci.* **2004**, *108–109*, 207–226.
- (3) Middelberg, A. P. J.; He, L.; Dexter, A. F.; Shen, H.-H.; Holt, S. A.; Thomas, R. K. The interfacial structure and Young's modulus of peptide films having switchable mechanical properties. *J. R. Soc., Interface* **2008**, *5*, 47–54.
- (4) Cattozzi, B.; de Vos, W. M.; Cosgrove, T.; Crossman, M.; Prescott, S. W. Manipulating interfacial polymer structures through mixed surfactant adsorption and complexation. *Langmuir* **2012**, *28*, 6282–6290.
- (5) Cattozzi, B.; de Vos, W. M.; Cosgrove, T.; Crossman, M.; Espidel, Y.; Prescott, S. W. Interpolymer complexation: comparisons of bulk and interfacial structures. *Langmuir* **2015**, *31*, 4151–4159.
- (6) Woodward, A.; Cosgrove, T.; Espidel, J.; Jenkins, P.; Shaw, N. Monodisperse emulsions from a microfluidic device, characterised by diffusion NMR. *Soft Matter* **2007**, *3*, 627–633.
- (7) Nazir, H.; Zhang, W.; Liu, Y.; Chen, X.; Wang, L.; Naseer, M. M.; Ma, G. Silicone oil emulsions: Strategies to improve their stability and applications in hair care products. *International J. Cosmet. Sci.* **2014**, *36*, 124–133.
- (8) Clifton, B.; Cosgrove, T.; Richardson, R.; Zarbakhsh, A.; Webster, J. The structure of block copolymers at the fluid/fluid interface. *Phys. B* **1998**, *248*, 289–296.
- (9) Schlossman, M. L. Liquid-liquid interfaces: studied by X-ray and neutron scattering. *Curr. Opin. Colloid Interface Sci.* **2002**, *7*, 235–243.
- (10) Wei, Z.; Prescott, S. W. Scattering approaches to probing surface layers under confinement. *Curr. Opin. Colloid Interface Sci.* **2015**, *20*, 253–260.
- (11) Phipps, J. S.; Richardson, R. M.; Cosgrove, T.; Eaglesham, A. Neutron reflection studies of copolymers at the hexane/water interface. *Langmuir* **1993**, *9*, 3530–3537.
- (12) Zarbakhsh, A.; Querol, A.; Bowers, J.; Webster, J. R. P. Structural studies of amphiphiles adsorbed at liquid-liquid interfaces using neutron reflectometry. *Faraday Discuss.* **2005**, *129*, 155–167.
- (13) Scoppola, E.; Watkins, E.; Li Destri, G.; Porcar, L.; Campbell, R. A.; Konovalov, O.; Fragneto, G.; Diat, O. Structure of a liquid/liquid interface during solvent extraction combining X-ray and neutron reflectivity measurements. *Phys. Chem. Chem. Phys.* **2015**, *17*, 15093–15097.
- (14) Lu, J. R.; Li, Z. X.; Smallwood, J.; Thomas, R. K.; Penfold, J. Detailed structure of the hydrocarbon chain in a surfactant monolayer at the air/water interface: neutron reflection from hexadecyltrimethylammonium bromide. *J. Phys. Chem.* **1995**, *99*, 8233–8243.
- (15) Lu, J. R.; Purcell, I. P.; Lee, E. M.; Simister, E. A.; Thomas, R. K.; Rennie, A. R.; Penfold, J. The composition and structure of sodium dodecyl sulfate-dodecanol mixtures adsorbed at the air-water interface: a neutron reflection study. *J. Colloid Interface Sci.* **1995**, *174*, 441–455.
- (16) Zarbakhsh, A.; Webster, J. R. P.; Wojciechowski, K. Neutron reflectivity study of alkylated azacrown ether at the air-liquid and the liquid-liquid interfaces. *Langmuir* **2009**, *25*, 11569–11575.
- (17) Zarbakhsh, A.; Querol, A.; Bowers, J.; Yaseen, M.; Lu, J. R.; Webster, J. R. P. Neutron reflection from the liquid-liquid interface: Adsorption of hexadecylphosphorylcholine to the hexadecane - Aqueous solution interface. *Langmuir* **2005**, *21*, 11704–11709.
- (18) Campana, M.; Webster, J. R. P.; Lawrence, M. J.; Zarbakhsh, A. Structural conformation of lipids at the oil-water interface. *Soft Matter* **2012**, *8*, 8904.
- (19) Knock, M. M.; Bell, G. R.; Hill, E. K.; Turner, H. J.; Bain, C. D. Sum-frequency spectroscopy of surfactant monolayers at the oil-water interface. *J. Phys. Chem. B* **2003**, *107*, 10801–10814.
- (20) Schlossman, M. L. X-ray scattering from liquid-liquid interfaces. *Phys. B* **2005**, *357*, 98–105.
- (21) Wojciechowski, K.; Gutberlet, T.; Tikhonov, A.; Kashimoto, K.; Schlossman, M. X-ray reflectivity study of the adsorption of azacrown ether at liquid-liquid interface. *Chem. Phys. Lett.* **2010**, *487*, 62–66.
- (22) Pershan, P. S.; Schlossman, M. *Liquid Surfaces and Interfaces: Synchrotron X-ray Methods*; Cambridge University Press, 2012.
- (23) Bu, W.; Mihaylov, M.; Amoanu, D.; Lin, B.; Meron, M.; Kuzmenko, I.; Soderholm, L.; Schlossman, M. L. X-ray studies of interfacial strontium-extractant complexes in a model solvent extraction system. *J. Phys. Chem. B* **2014**, *118*, 12486–12500.
- (24) Scoppola, E.; Watkins, E. B.; Campbell, R. A.; Konovalov, O.; Girard, L.; Dufrêche, J. F.; Ferru, G.; Fragneto, G.; Diat, O. Solvent extraction: structure of the liquid-liquid interface containing a diamide ligand. *Angew. Chem., Int. Ed.* **2016**, *55*, 9326–9330.
- (25) Prestidge, C. A.; Barnes, T.; Simovic, S. Polymer and particle adsorption at the PDMS droplet-water interface. *Adv. Colloid Interface Sci.* **2004**, *108–109*, 105–118.
- (26) Dexter, A. F.; Malcolm, A. S.; Middelberg, A. P. J. Reversible active switching of the mechanical properties of a peptide film at a fluid-fluid interface. *Nat. Mater.* **2006**, *5*, S02–S06.
- (27) Zeng, B. J.; Chuan, Y. P.; O'Sullivan, B.; Caminschi, I.; Lahoud, M. H.; Thomas, R.; Middelberg, A. P. J. Receptor-specific delivery of protein antigen to dendritic cells by a nanoemulsion formed using top-down non-covalent click self-assembly. *Small* **2013**, *9*, 3736–3742.
- (28) He, L.; Malcolm, A. S.; Dimitrijev, M.; Onaizi, S. A.; Shen, H. H.; Holt, S. A.; Dexter, A. F.; Thomas, R. K.; Middelberg, A. P. J. Cooperative tuneable interactions between a designed peptide biosurfactant and positional isomers of SDOBS at the air–water interface. *Langmuir* **2009**, *25*, 4021–4026.
- (29) Borah, D.; Rasappa, S.; Sentharamakannan, R.; Kosmala, B.; Shaw, M. T.; Holmes, J. D.; Morris, M. A. Orientation and alignment control of microphase-separated PS-b-PDMS Substrate Patterns via Polymer Brush Chemistry. *Appl. Mater. Interfaces* **2012**, *5*, 88–97.
- (30) Nečas, D.; Klapetek, P. Gwyddion: an open-source software for SPM data analysis. *Cent. Eur. J. Phys.* **2012**, *10*, 181–188.
- (31) Brittain, W. J.; Minko, S. A structural definition of polymer brushes. *J. Polym. Sci., Part A: Polym. Chem.* **2007**, *45*, 3505–3512.
- (32) James, M.; Nelson, A.; Holt, S. A.; Saerbeck, T.; Hamilton, W. A.; Klose, F. The multipurpose time-of-flight neutron reflectometer "Platypus" at Australia's {OPAL} reactor. *Nucl. Instrum. Methods Phys. Res., Sect. A* **2011**, *632*, 112–123.
- (33) Bahri, M. A.; Hoebke, M.; Grammenos, A.; Delanaye, L.; Vandewalle, N.; Seret, A. Investigation of SDS, DTAB and CTAB micelle viscosities by electron spin resonance. *Colloids Surfaces., A* **2006**, *290*, 206–212.
- (34) Prosser, A. J.; Franses, E. I. Adsorption and surface tension of ionic surfactants at the air-water interface: Review and evaluation of equilibrium models. *Colloids Surf., A* **2001**, *178*, 1–40.
- (35) Penfold, J.; Thomas, R. K.; Simister, E. A.; Lee, E. M.; Rennie, A. R. The Structure of Mixed Surfactant Monolayers at the Air-Liquid Interface, as Studied by Specular Neutron Reflection. *J. Phys.: Condens. Matter* **1990**, *2*, SA411–SA416.
- (36) Tayeb, H. H.; Piantavigna, S.; Howard, C. B.; Nouwens, A.; Mahler, S. M.; Middelberg, A. P. J.; He, L.; Holt, S. A.; Sainsbury, F. Insights into the interfacial structure-function of poly(ethylene glycol)-decorated peptide-stabilised nanoscale emulsions. *Soft Matter* **2017**, *13*, 7953–7961.
- (37) Jacrot, B.; Zaccai, G. Determination of molecular weight by neutron scattering. *Biopolymers* **1981**, *20*, 2413–2426.

- (38) Nelson, A. Co-refinement of multiple-contrast neutron/X-ray reflectivity data using MOTOFIT. *J. Appl. Crystallogr.* **2006**, *39*, 273–276.
- (39) Purcell, I. P.; Lu, J. R.; Thomas, R. K.; Howe, A. M.; Penfold, J. Adsorption of sodium dodecyl sulfate at the surface of aqueous solutions of poly(vinylpyrrolidone) studied by neutron reflection. *Langmuir* **1998**, *14*, 1637–1648.
- (40) Fragneto, G.; Thomas, R. K.; Rennie, A. R.; Penfold, J. Neutron reflection from hexadecyltrimethylammonium bromide adsorbed on smooth and rough silicon surfaces. *Langmuir* **1996**, *12*, 6036–6043.
- (41) Sauerbrey, G. Verwendung von Schwingquarzen zur Wägung dünner Schichten und zur Mikrowägung. *Z. Phys.* **1959**, *155*, 206–222.
- (42) Lee, J. N.; Park, C.; Whitesides, G. M. Solvent Compatibility of Poly(dimethylsiloxane)-Based Microfluidic Devices. *Anal. Chem.* **2003**, *75*, 6544–6554.
- (43) Lu, J. R.; Simister, E. A.; Lee, E. M.; Thomas, R. K.; Rennie, A. R.; Penfold, J. Direct determination by neutron reflection of the penetration of water into surfactant layers at the air/water interface. *Langmuir* **1992**, *8*, 1837–1844.
- (44) Lu, J. R.; Simister, E. A.; Thomas, R. K.; Penfold, J. Adsorption of alkyltrimethyl ammonium bromide at the air-water interface. *Prog. Colloid Polym. Sci.* **1993**, *92*–97.
- (45) Ducker, W. A.; Wanless, E. J. Adsorption of hexadecyltrimethylammonium bromide to mica: nanometer-scale study of binding-site competition effects. *Langmuir* **1999**, *15*, 160–168.
- (46) Penfold, J.; et al. Recent advances in the study of chemical surfaces and interfaces by specular neutron reflection. *J. Chem. Soc., Faraday Trans.* **1997**, *93*, 3899–3917.
- (47) Wang, R.; Wang, Z.-G. Effects of image charges on double layer structure and forces. *J. Chem. Phys.* **2013**, *139*, No. 124702.
- (48) Cherstvy, A. G.; Winkler, R. G. Polyelectrolyte adsorption onto oppositely charged interfaces: Image-charge repulsion and surface curvature. *J. Phys. Chem. B* **2012**, *116*, 9838–9845.
- (49) Lu, J. R.; Thomas, R. K.; Aveyard, R.; Binks, B. P.; Cooper, P.; et al. Structure and Composition of dodecane layers spread on aqueous solutions of C14TAB: neutron reflection and surface tension measurements. *J. Phys. Chem.* **1992**, *96*, 10971–10978.
- (50) Purcell, I. P.; Thomas, R. K.; Penfold, J.; Howe, A. M. Adsorption of SDS and PVP at the air/water interface. *Colloids Surf., A* **1995**, *94*, 125–130.
- (51) Cooke, D. J.; Dong, C. C.; Lu, J. R.; Thomas, R. K.; Simister, E. A.; Penfold, J. Interaction between polyethyleneoxide and sodium dodecyl sulfate studied by neutron reflection. *J. Phys. Chem. B* **1998**, *102*, 4912–4917.
- (52) Staples, E.; Penfold, J.; Tucker, I. Adsorption of mixed surfactants at the oil-water interface. *J. Phys. Chem. B* **2000**, *104*, 606–614.
- (53) Schweighofer, K. J.; Essmann, U.; Berkowitz, M. Simulation of sodium dodecyl sulfate at the water-vapor and water-carbon tetrachloride interfaces at low surface coverage. *J. Phys. Chem. B* **1997**, *101*, 3793–3799.
- (54) Dominguez, H.; Berkowitz, M. L. Computer simulations of sodium dodecyl sulfate at liquid/liquid and liquid/vapor interfaces. *J. Phys. Chem. B* **2000**, *104*, 5302–5308.
- (55) Turner, S. F.; Clarke, S. M.; Rennie, A. R.; et al. Adsorption of sodium dodecyl sulfate to a polystyrene/water interface studied by neutron reflection and attenuated total reflection infrared spectroscopy. *Langmuir* **1999**, *15*, 1017–1023.
- (56) Rodahl, M.; Höök, F.; Fredriksson, C.; Keller, C. A.; Krozer, A.; Brzezinski, P.; Voinova, M.; Kasemo, B. Simultaneous frequency and dissipation factor QCM measurements of biomolecular adsorption and cell adhesion. *Faraday Discuss.* **1997**, *107*, 229–246.
- (57) Fragneto, G.; Lu, J. R.; McDermott, D. C.; Thomas, R. K.; Rennie, A. R.; Gallagher, P. D.; Satija, S. K. Structure of Monolayers of Tetraethylene Glycol Monododecyl Ether Adsorbed on Self-Assembled Monolayers on Silicon: A Neutron Reflectivity Study. *Langmuir* **1996**, *12*, 477–486.
- (58) Thirtle, P. N.; Li, Z. X.; Thomas, R. K.; Rennie, A. R.; et al. Structure of nonionic surfactant layers adsorbed at the solid/liquid interface on self-assembled monolayers with different surface functionality: A neutron reflection. *Langmuir* **1997**, *13*, 5451–5458.
- (59) Manne, S.; Cleveland, J. P.; Gaub, H. E.; Stucky, G. D.; Hansma, P. K. Direct visualization of surfactant hemimicelles by force microscopy of the electrical double layer. *Langmuir* **1994**, *10*, 4409–4413.
- (60) Tiberg, F.; Brinck, J.; Grant, L. Adsorption and surface-induced self-assembly of surfactants at the solid-aqueous interface. *Curr. Opin. Colloid Interface Sci.* **1999**, *4*, 411–419.
- (61) Bandyopadhyay, S.; Shelley, J. C.; Tarek, M.; Moore, P. B.; Klein, M. L. Surfactant aggregation at a hydrophobic surface. *J. Phys. Chem. B* **1998**, *102*, 6318–6322.
- (62) Holt, S. A.; Reynolds, P. A.; White, J. W. Growth of silicated films at the solid/liquid interface. *Phys. Chem. Chem. Phys.* **2000**, *2*, 5667–5671.
- (63) Levchenko, A. A.; Argo, B. P.; Vidu, R.; Talroze, R. V.; Stroeve, P. Kinetics of sodium dodecyl sulfate adsorption on and desorption from self-assembled monolayers measured by surface plasmon resonance. *Langmuir* **2002**, *18*, 8464–8471.
- (64) Wanless, E. J.; Ducker, W. A. Organization of sodium dodecyl sulfate at the graphite-solution interface. *J. Phys. Chem.* **1996**, *100*, 3207–3214.